Sciencexpress Research Articles

Neuronal Activity Promotes Oligodendrogenesis and Adaptive Myelination in the Mammalian Brain

Erin M. Gibson,[1]* David Purger,[1,2]* Christopher W. Mount,[1,3] Andrea K. Goldstein,[1] Grant L. Lin,[1,3] Lauren S. Wood,[1] Ingrid Inema,[1] Sarah E. Miller,[1] Gregor Bieri,[3] J. Bradley Zuchero,[4] Ben A. Barres,[4] Pamelyn J. Woo,[1] Hannes Vogel,[5] Michelle Monje[1]†

[1]Departments of Neurology, Neurosurgery and Pediatrics, Institute for Stem Cell Biology and Regenerative Medicine, Stanford University School of Medicine, Stanford, CA, USA. [2]Graduate Program in Stem Cell Biology and Regenerative Medicine, Stanford University School of Medicine, Stanford, CA, USA. [3]Graduate Program in Neuroscience, Stanford University School of Medicine, Stanford, CA, USA. [4]Departments of Neurobiology and Developmental Biology, Stanford University School of Medicine, Stanford, CA, USA. [5]Department of Pathology, Stanford University School of Medicine, Stanford, CA, USA.

*These authors contributed equally to this work.

†Corresponding author. E-mail: mmonje@stanford.edu

Myelination of the central nervous system requires the generation of functionally mature oligodendrocytes from oligodendrocyte precursor cells (OPC). Electrically active neurons may influence OPC function and selectively instruct myelination of an active neural circuit. Here we use optogenetic stimulation of premotor cortex in awake, behaving mice to demonstrate that neuronal activity elicits a mitogenic response of neural progenitor cells and OPCs, promotes oligodendrogenesis and increases myelination within the deep layers of the premotor cortex and subcortical white matter. We further show that this neuronal activity-regulated oligodendrogenesis and myelination is associated with improved motor function of the corresponding limb. Oligodendrogenesis and myelination appear necessary for the observed functional improvement, as epigenetic blockade of oligodendrocyte differentiation and myelin changes prevents the activity-regulated behavioral improvement.

Development of the myelinated fiber infrastructure of the brain occurs throughout childhood and young adulthood and is classically thought to complete when the frontal lobes finish myelin formation in the fourth decade of human life (*1*, *2*). Maturation of the complex neural circuitry necessary for high-level cognitive and motor functions depends on myelination, the process by which oligodendrocytes ensheathe and insulate axons to facilitate fast, saltatory conduction of electrical impulses. While the protracted nature of neocortical myelination is well recognized, the mechanisms governing myelination after infancy remain largely unknown (*1*, *3*, *4*).

An intriguing but unproven possibility is that postnatal myelination may be modulated by mature neurons in order to augment an active circuit. The idea that excitatory neuronal activity instructs myelination, including OPC proliferation, differentiation and myelin biosynthesis, is supported by multiple lines of evidence. Blockade of activity in the developing optic nerve by axotomy or tetrodotoxin decreases OPC proliferation (*5*), myelination in vitro is activity-dependent (*6–9*), and some data suggest that OPC proliferation, differentiation or the rate of myelin development in vivo is enhanced by non-physiological (333 Hz) or pathological perturbations of electrical activity (*10*, *11*). Further supporting the idea that excitatory neuronal activity may influence OPC behavior, neurons form glutamatergic synaptic connections onto OPCs (*12–17*). However, an elegant study conditionally ablating a necessary subunit of the NMDA receptor in oligodendroglial lineage cells during development did not demonstrate deficits in oligodendrogenesis or myelination, arguing against a role for direct NMDA receptor-mediated axoglial synaptic neurotransmission as a mechanism regulating myelination in vivo (*18*). The potential role of neuronal activity in the regulation of myelin-forming cells remains unclear in vivo, and, if established, would constitute a previously underappreciated mechanism by which experience directs adaptive behavioral change.

Results

Description of the Optogenetic Model and Experimental Paradigm

Here, we test the effects of neuronal activity on oligodendroglial cells in vivo using optogenetic stimulation of premotor cortex in awake, behaving Thy1::channelrhodopsin (ChR2) mice (*19*, *20*). In this well-characterized model the excitatory opsin is expressed in a subset of neurons under the control of the Thy1 promoter. In the cortex, the Thy1 promoter and thus the excitatory opsin are expressed chiefly in cortical layer V projection neurons and are not expressed in glial cell types (*19*, *20*). ChR2-expressing neurons respond to pulses of blue (470 nm) light with millisecond precision such that the frequency of light pulses elicits neuronal spiking of the same frequency (*19*, *20*). Expression of ChR2 does not alter the electrical properties of neurons in the absence of blue light and does not affect neuronal survival under basal conditions or with blue light stimulation using standard experimental parameters (*21*). When the optical fiber is placed just below the pial surface, approximately 10% of the blue light penetrates 0.5 mm, or about halfway through the cortex, and approximately 1% reaches 1 mm (to cortical layer VI) (*22*). This stimulates the apical dendrites of layer V neurons and, to a lesser extent as the light is attenuated by layer V, the neuronal somata, resulting in neuronal firing of layer V projection neurons (*22*). Heat generated by this system is negligible under these conditions and localized to the optical fiber (*22*). Stimulating from just below the pial surface limits hardware-related injury to the skull and cortical layer I, in contrast to alternative strategies such as intracortical microstimulation (ICMS) that involve more extensive electrode-related tissue damage.

We placed the optical-neural interface just below the pial surface in cortical layer I of area M2 (premotor area; Fig. 1A) in juvenile (P35) mice and stimulated unilaterally with blue light for 30-s intervals every two minutes over a 30-min period at 20 Hz, a frequency consistent with the 10–40 Hz physiological firing rates of layer V projection neurons in motor cortex (*19*). Unilateral stimulation of right-sided M2, a high level cortical region involved in motor planning and the generation of complex and goal-directed motor behavior (*23*), caused mice to ambulate consistently in the contralateral (left) direction when the blue light was on (movie S1); this behavioral measure confirms proper placement of the light stimulation fiber and demonstrates the expected behavioral consequences of optogenetic premotor cortex stimulation.

The placement of the fiber requires breaching the skull and dura, and

the optical fiber penetrates the most superficial layer of cortex (layer I). Because injury (*24*) and the associated microglial inflammation (*25*) can influence OPC behavior, wild-type (WT, no opsin present) littermate control animals were identically manipulated to control for effects of surgery, fiber placement and light. In WT mice, blue light stimulation causes no observable change in behavior. Manipulated WT littermate controls were utilized in all analyses described below to account for effects of injury and inflammation.

Neuronal Activity-Regulated Precursor Cell Proliferation

To test the acute effects of neuronal activity on cell proliferation, we administered the thymidine analog EdU (5-ethynyl-2′-deoxyuridine) at the beginning of the 30-min stimulation period to label dividing cells and sacrificed mice three hours later. Following this period of activity, we observed a proliferative response in premotor cortex (Fig. 1, A and B) and subcortical white matter projections in the corpus callosum (Fig. 2). At P35, we observed a 4-fold increase in dividing cells in stimulated (ipsilateral) M2 compared to manipulated WT littermate controls (7368 cells ± 1228 cells vs. 1940 cells ± 512; n = 3/group; $P < 0.001$; Fig. 1C). Dividing cells, outside the immediate area of optical fiber placement in layer I, were found in the deep cortical layers near the optogenetically-stimulated neurons and in the subcortical fibers of the corpus callosum (Figs. 1B and 2).

To characterize the cells proliferating in response to neuronal activity, we employed immunofluorescence staining for cell identity markers (Fig. 1, D and E, and fig. S1). We found that 54% of the dividing cells in optogenetically-stimulated Thy1::ChR2 M2 express the oligodendroglial lineage marker Olig2; stimulated M2 in Thy1::ChR2 mice exhibited a significant increase in dividing Olig2$^+$ cells compared to WT controls (4032 ± 832 vs. 519 ± 152 cells, respectively; $P < 0.001$; Fig. 1D); 24.5% of the dividing cells were PDGFRα$^+$ OPCs (Fig. 1E); a similar number of EdU-marked OPCs was detected by co-labeling with Sox2 and Olig2 (fig. S1B). A significant increase in EdU-marked Sox2$^+$ neural precursor cells (NPC) (*26*) was also observed in stimulated M2 compared to WT controls (fig. S1A). No significant fraction of the proliferating cells represented GFAP$^+$ or S100β$^+$ astrocytes (fig. S1, C and D). Consistent with reports that optogenetic stimulation of ChR2-expressing neurons within the parameters used here does not induce neuronal injury or death (*21*), cleaved caspase-3 staining, indicating apoptotic cells, was not observed within optogenetically-stimulated M2 (fig. S2).

An increase in proliferation was also observed in the corpus callosum of Thy1::ChR2 mice compared to manipulated WT controls (Fig. 2). While EdU labeling was observed throughout the corpus callosum, a defined region subjacent to motor cortex and distant from the ventricular region was quantified to avoid the potential confound of EdU$^+$ cells arising from the periventricular/subventricular zone which contains a briskly mitotic and migratory population of cells that take up the EdU marker but may be distinct from those cells responding to neuronal activity (Fig. 2A). Total EdU$^+$ cell quantification revealed a two-fold increase in dividing cells in the stimulated Thy1::ChR2 animals compared to manipulated WT controls (2440 ± 174 cells vs. 916 ± 77; n = 3/group; $P < 0.0001$; Fig. 2, B and C), with a significant increase in EdU-marked Olig2$^+$ oligodendroglial lineage cells in the stimulated Thy1::ChR2 animals compared to manipulated WT controls (1016 ± 68 cells vs. 455 ± 58, n = 3/group; $P < 0.0001$; Fig. 2D). Similar to M2, approximately half (42%) of the dividing cells are Olig2$^+$ (Fig. 2D), and no EdU-labeled GFAP$^+$ astrocytes or EdU-labeled S100β$^+$ astrocytes were found.

Optogenetic stimulation of opsin-expressing neurons in motor cortex elicits expected electrophysiological and behavioral responses (*19*, *20*), but one cannot exclude the possibility of decreased neuronal health due to the presence of the opsin or to the optogenetic stimulation of firing. To control for the effects of pathological neuronal activity, we induced generalized tonic-clonic motor seizures optogenetically using the same frequency and intensity of stimulation but placing the optical fiber more medially in M2 so that light stimulates both motor cortices simultaneously. Proliferation comparable to that seen in the manipulated WT control animals was observed in the seizure animals (Fig. 1C) but not to the degree seen in animals following optogenetic stimulation that results in complex motor behavioral output (n = 3; $P < 0.001$; Fig. 1, C to E). That optogenetically-induced motor seizures did not elicit a proliferative response of the same magnitude indicates that pathological neuronal activity is not sufficient to account for the observed proliferative effect. Taken together, these findings show that moderate, precisely timed levels of electrical activity in neurons evoking naturalistic behavior in awake, freely-behaving mice promoted the proliferation of neural precursor and oligodendroglial precursor cell populations.

Evaluation of Inflammatory Response to Fiber Optic Manipulation

Given the effects of microglial inflammation on NPC (*27–29*) and OPC (*25*) proliferation and differentiation, the microglial response must be carefully evaluated and accounted for in this model. The majority of EdU$^+$ microglia were localized to the superficial layers of M2 near the site of the optical fiber and less in the deep layers of cortex where the optogenetically-stimulated neuronal somata reside (Fig. 3, A and B). Approximately 75% of the dividing activated microglia were localized to superficial cortex, while only 25% were found in deep cortical layers in all experimental groups (Fig. 3B). To be conservative, as microglial effects such as cytokine secretion could be exerted over some distance, we quantified all microglia in M2 up to cortical layer I, excluding only those within approximately 100 μm of the optical fiber (Fig. 3, A to F). Consistent with the injury induced by the manipulation, we observed a significant increase in EdU-labeled dividing microglia marked by the pan-microglial marker Iba1 (*30*, *31*) and the marker of microglial "activation" CD68 (*32*, *33*) compared to the contralateral hemisphere in both WT and Thy1::ChR2 mice, as well as in the seizure control animals ($P < 0.05$ in all comparisons; Fig. 3, C and D). Reassuringly, the number of EdU$^+$/Iba1$^+$/CD68$^+$ activated microglia was not different between optogenetically stimulated Thy1::ChR2 and manipulated WT mice at the 3 hour time point (1991 ± 107 vs. 1412 ± 377, P = 0.10, Fig. 3D). Seizure animals exhibited an equivalent number of EdU$^+$/Iba1$^+$/CD68$^+$ microglia compared to Thy1::ChR2 mice in whom locomotion was induced and compared to manipulated WT controls (Fig. 3D). By 24 hours, EdU-marked Iba1$^+$/CD68$^+$ activated microglia were significantly decreased in premotor cortex compared to the three hour time point (1991 ± 107 at three hours vs. 801 ± 181 at 24 hours for Thy1::ChR2 animals; n = 3; P = 0.005; Fig. 3D). There was no difference in the numbers of EdU$^+$/Iba1$^+$/CD68$^+$ activated microglia in stimulated Thy1::ChR2 compared to manipulated WT mice at 24 hours (801 ± 181 vs. 515 ± 147; n = 3; P = 0.07; Fig. 3D). The overall density (EdU$^+$ and EdU$^-$) of activated Iba1$^+$/CD68$^+$ microglia was also not different between Thy1::ChR2 and WT at three hours or 24 hours, indicating an equal microglial inflammatory response in manipulated Thy1::ChR2 and WT littermate control mice ($P > 0.25$ in all comparisons; Fig. 3E). In the corpus callosum, no EdU-marked, CD68$^+$ activated microglia were detected in either stimulated (or unstimulated) Thy1::ChR2 or WT mice (Fig. 2, B and E). The microglial inflammatory response was also evaluated following a 7-day stimulation paradigm (cycles of 30 s on, 2 min off over 10 min each day; see below). The overall density (EdU$^+$ and EdU$^-$) of activated Iba1$^+$/CD68$^+$ microglia was also not different between Thy1::ChR2 and WT on day 7 of or 4 weeks following this 7-day stimulation paradigm (Fig. 3F). The microglial inflammatory response, predominantly localized to the superficial cortex, is thus equal in Thy1::ChR2 mice compared to WT littermate controls following optical fiber placement and blue light stimulation in this model.

Neuronal Activity-Regulated Oligodendrocyte Differentiation

To define the population dynamics and fate of cells dividing in response to neuronal activity, we repeated the above experiment but sacrificed P35 mice at 24 hours after a single session of optogenetic stimulation, and in a parallel cohort sacrificed at four weeks following a 7-day stimulation paradigm (cycles of 30 s on, 2 min off over 10 min each day, resulting in 2.5 min of total stimulation daily). In Thy1::ChR2 mice, we observed no statistically significant change in the total number of EdU^+ cells from three to 24 hours, and only 1-2% of EdU^+ cells co-labeled with either Ki67 or cleaved caspase-3, indicating that the dividing cells cease proliferation soon after stimulated neuronal activity and survive in the subacute time period ($n = 3$; Fig. 4, A and B). In contrast, 32% of the EdU^+ cells in WT animals remained in a proliferative state at 24 hours, evidenced by co-labeling with Ki67 ($n = 3$; $P < 0.05$; Fig. 4B). Thy1::ChR2 mice have fewer EdU^+ cells present in M2 at four weeks, which may be due to cell dispersion and death during that interval ($n = 7$/group; Fig. 4A and fig. S3A).

Dividing cells were localized to motor cortex and subcortical white matter including the corpus callosum three hours after neuronal activity (Figs. 1B and 2). By four weeks, dispersion of EdU^+ cells was observed (fig. S3A), but no significant increase in EdU^+ cells was observed in the corresponding corticospinal tract at the level of the cervical spinal cord compared to the contralateral side ($n = 4$ Thy1::ChR2, $P = 0.48$) or to WT ($n = 3$ WT; $P = 0.16$; fig. S3, B and C). This localization may reflect differences inherent in cortical OPCs compared to those found in the deep white matter (*34*, *35*), proximity to neuronal cell bodies (*36*), or differences in neuronal cell types (e.g., callosal projection neurons vs. corticofugal projection neurons).

Because changes in the epigenetic landscape of NPCs and OPCs are necessary for progression to differentiated states (*37*, *38*), we examined population-level changes in histone modifications (Fig. 4, C and D). We found a neuronal activity-regulated increase in trimethylation of histone H3 lysine 9 (indicative of a repressive, heterochromatin state; $P < 0.05$) and a concomitant decrease in acetylated histone H3 (correlating with activating regulatory elements; $P < 0.05$) in dividing (EdU^+) cells between three and 24 hours following optogenetically-stimulated neuronal activity in Thy1::ChR2 mice (Fig. 4, C and D). Thus, neuronal activity promotes transition to a repressive chromatin state consistent with differentiation.

To evaluate the fate of the cells proliferating in response to neuronal activity, we optogenetically stimulated M2 daily as above for 7 days, then sacrificed mice four weeks after the end of stimulation ($n = 7$/group). In stimulated M2, we found the absolute number of newly generated (EdU^+) $Sox2^+/Olig2^-$ NPCs and oligodendroglial ($Olig2^+$) cells remained increased compared to manipulated WT controls ($P < 0.05$ for NPCs; $P < 0.01$ for $Olig2^+$; fig. S4 and Fig. 5A). Neuronal activity-regulated oligodendrogenesis is evidenced by an increase in the number of both EdU^+ early oligodendroglial cells expressing transcription factor Olig1 in a nuclear pattern ($Olig1^{nuclear+}$) and in EdU^+ mature oligodendrocytes expressing Olig1 in a perinuclear pattern ($Olig1^{perinuclear+}$) compared to manipulated WT control ($P < 0.05$ for nuclear Olig1 and $P < 0.05$ for perinuclear Olig1; Fig. 5, C and D) (*39*). Neuronal activity-regulated oligodendrogenesis was confirmed using CC1, also a marker for mature oligodendrocytes (534 ± 131 $EdU^+/CC1^+$ cells vs. 39 ± 30 cells; $n = 4$ Thy1::ChR2 mice, 3 WT mice; $P < 0.01$; Fig. 5, E and F). Supporting the interpretation that the cells dividing in response to neuronal activity had differentiated into oligodendrocytes, the EdU^+ OPC population ($EdU^+/PDGFR\alpha^+$ and $EdU^+/Sox2^+/Olig2^+$) had diminished compared to the acute time point (Fig. 5B and fig. S4B) concomitantly with the appearance of EdU^+ oligodendrocytes (Fig. 5, C to F). An increase in newly generated oligodendrocytes was also found in the corpus callosum of optogenetically stimulated Thy1::ChR2 mice as compared to identically manipulated WT littermate controls (162 ± 39 $EdU^+/CC1^+$ cells vs. 36 ± 19 cells; $n = 4$ Thy1::ChR2 mice, 3 WT mice; $P < 0.05$; Fig. 2F). These results demonstrate activity-regulated oligodendrogenesis within the active neural circuit.

Histone deacetylation is required for oligodendrocyte differentiation (*37*, *38*). Blockade of histone deacetylation with trichostatin A (TSA), an inhibitor of histone deacetylases (HDAC) 1 and 2, prevented new mature oligodendrocyte production assessed with $Olig1^{perinuclear}$ and CC1 markers ($n = 4$/group; $P = 0.49$ for $Olig1^{perinuclear}$ and $P = 0.44$ for CC1; Fig. 5, C to F). TSA administration had no effect on the total number of EdU-labeled cells detected at four weeks following stimulation ($P = 0.3$; fig. S5). Consistent with epigenetic blockade of differentiation, an increase in the number of EdU-labeled, $Olig1^{nuclear+}$ cells representing immature oligodendrocytes was observed at four weeks post stimulation ($P < 0.01$; Fig. 5D).

Response of Oligodendroglial Lineage Cells to Neuronal Activity in Adults

Using the same model, we evaluated the effect of neuronal activity on oligodendroglial lineage cells in adult animals. At 4 weeks following the 7-day paradigm of optogenetic stimulation (commencing at age P84), we found a two-fold increase in the total number of EdU-marked cells in the stimulated M2 compared to manipulated WT controls (2306 cells ± 337 vs. 983 ± 382; $n = 4$ Thy1::ChR2 mice, 3 WT mice; $P < 0.05$). There was a significant increase in the number of $Olig2^+$, EdU-marked cells in both M2 (788 ± 45 vs. 204 ± 71; $n = 4$ Thy1::ChR2 mice, 3 WT mice; $P < 0.0001$; fig. S6B) and in the corpus callosum (79 ±17 vs. 20 ± 9; $n = 4$ Thy1::ChR2 mice, 3 WT mice; $P < 0.05$; fig. S7B) of stimulated Thy1::ChR2 mice compared to identically-manipulated WT controls. Concomitant with a decrease in EdU-marked OPCs (figs. S6C and S7C), mature oligodendrocytes marked by EdU were increased 4 weeks following the end of the stimulation paradigm in adult animals. In M2, an increase in $EdU^+/CC1^+$ mature oligodendrocytes was found in optogenetically stimulated Thy1::ChR2 mice compared to manipulated WT littermates (767 ± 106 vs. 72 ± 50; $n = 4$ Thy1::ChR2 mice, 3 WT mice; $P < 0.001$; fig. S6D). Similarly, an increase in EdU-marked mature oligodendrocytes was observed in the adult corpus callosum (112 ± 32 $EdU^+/CC1^+$ cells vs. 7 ± 4 $EdU^+/CC1^+$ cells; $n = 4$ Thy1::ChR2 mice, 3 WT mice, respectively; $P < 0.05$; fig. S7D).

As above, EdU-marked, newly generated oligodendrocytes were quantified in premotor cortex and in corpus callosum following optogenetic stimulation at P35 or P84. Adjusting the total number of $EdU^+/CC1^+$ cells for the volume of tissue analyzed, we found more $EdU^+/CC1^+$ cells per mm^3 in the corpus callosum compared to M2 in mice stimulated at P35 (8983 ± 2188 cells/mm^3 in corpus callosum vs. 3010 ± 737 cells/mm^3 in M2; $n = 4$ Thy1::ChR2 mice; $P < 0.05$; fig. S8A). In animals stimulated at P84, a more comparable number of newly generated oligodendrocytes per tissue volume was found (6214 ± 1763 cells/mm^3 in corpus callosum vs. 4318 ± 599 cells/mm^3 in M2; $n = 4$ Thy1::ChR2 mice; $P = 0.35$; fig. S8B).

Neuronal Activity-Regulated Myelination

Even small changes in the thickness of the myelin sheath relative to axon caliber (i.e., *g*-ratio) can have a profound effect on impulse conduction speed (*40*). To ascertain the effect of neuronal activity on myelin thickness, we used transmission electron microscopy (TEM) to analyze myelin thickness in M2 layer VI and subcortical fibers entering the corpus callosum four weeks after optogenetic stimulation (Fig. 6A). Relative to axonal diameter (*g*-ratio = axon diameter/axon + myelin sheath diameter), myelin sheaths were thicker (i.e., decreased *g*-ratio) in optogenetically-stimulated M2 and subcortical fibers ($g = 0.701 \pm 0.014$; $n = 4$ mice) compared to manipulated WT controls ($g = 0.756 \pm 0.003$; $n = 3$ mice; $P < 0.05$; Fig. 6B). No difference in *g*-ratio was observed between

genotypes on the side contralateral to stimulation (P = 0.13; Fig. 6C). Quantification of g-ratios was performed by two independent blinded raters.

As supportive evidence to the TEM studies above, we examined the expression of the myelin-related protein myelin basic protein (MBP). While MBP expression levels do not necessarily indicate the formation of compact myelin, as pre-myelinating oligodendrocytes express MBP, consistent with the TEM data above we found that MBP expression was also increased within M2 and subcortical white matter at four weeks following optogenetically-stimulated neuronal activity (n = 10 Thy1::ChR2, n = 9 WT; $P < 0.001$; fig. S9).

Behavioral Consequences

To evaluate possible functional consequences of neuronal activity-regulated oligodendrogenesis and myelination, we tested motor behavioral performance using CatWalk gait analysis four weeks following the 7-day stimulation paradigm, hypothesizing *a priori* that increased myelination would result in improvement of the sensitive measure of limb swing speed (*41*). The CatWalk gait analysis test does not require any prior training. CatWalk gait analysis (Fig. 7A) indicated improvement in swing speed of the correlate (left) forelimb during normal gait (inter-limb variation +4.8 ± 1.4 cm/s in Thy1::ChR2 mice vs. –4.3 ± 1.7 cm/s in WT mice; n = 5 Thy1::ChR2, n = 9 WT; $P < 0.05$; Fig. 7B), with no change in other parameters of gait such as forepaw strike intensity or stride length (Fig. 7, C and D). There was no effect of genotype on swing speed symmetry (inter-limb variation for unmanipulated mice –1.8 ± 4.0 cm/s vs. –1.2 ± 3.2 cm/s; n = 6 Thy1::ChR2, n = 6 WT, respectively; P = 0.58). Thus, oligodendrogenesis and increased myelin thickness in response to neuronal excitation correlates with altered motor function four weeks later.

Necessity of Myelin Changes

Do changes in myelin-forming cells account for the observed behavioral improvement? Neuronal activity could affect multiple parameters beyond oligodendrogenesis and myelination that are relevant to behavioral performance in the active circuit. One possibility is that asymmetric walking behavior led to asymmetric muscle development. However, we found that muscle mass and mean fiber diameter of the triceps and biceps brachii were unaffected by our protocol (n = 4/group; $P > 0.3$; fig. S10).

While muscle structure remains unaltered by the optogenetic stimulation paradigm, other activity-dependent changes in the motor circuit such as subtle alterations in synaptic strength could account for the observed behavioral improvement. To address this question, we used HDAC inhibition with TSA, a manipulation that would be expected to enhance synaptic plasticity (*42*, *43*) but to block oligodendrogenesis (*37*, *38*), reasoning that preventing the behavioral improvement in this context would argue for the necessity of activity-induced changes in myelin-forming cells. We thus blocked oligodendrogenesis to determine if it was necessary for the increase in correlate limb swing speed. We administered TSA concomitantly with optogenetic stimulation at P35 to block oligodendrogenesis epigenetically and measured both myelination by TEM and gait performance on the CatWalk four weeks post stimulation. TSA administration effectively blocked oligodendrogenesis (n = 4 Thy1::ChR2, n = 3 WT; $P < 0.05$; Fig. 5, D and F) and blocked the effect of neuronal activity on myelination (g-ratio = 0.756 ± 0.009 in stimulated, TSA-treated Thy1::ChR2 vs. 0.762 ± 0.008 in manipulated TSA-treated WT; n = 3/group; P = 0.62; Fig. 6D). The observed effect on myelin thickness could be due to HDAC inhibitor-mediated blockade of new oligodendrocyte differentiation, or due to effects of TSA on existing oligodendrocytes. Blockade of activity-regulated oligodendrogenesis and myelination prevented the behavioral effect (n = 6 Thy1::ChR2, n = 5 WT; P = 0.67; Fig. 7B). TSA administration did not affect baseline behavior or other parameters of gait (Fig. 7, C and D). As noted above, HDAC inhibition will affect many cell types, and an important consideration is whether TSA administration could itself negatively modulate motor function by effects on neurons or synaptic function. To the contrary, HDAC inhibition has been shown to improve learning and synaptic plasticity (*42*, *43*) and so effects of TSA on neuronal plasticity or function would not be expected to account for the blockade of improvement in motor function. These findings support the interpretation that oligodendrocyte differentiation and/or myelination are necessary for the motor behavioral improvement observed following neuronal activity in this model.

Discussion

The results presented here demonstrate that behaviorally-relevant neuronal activity in layer V projection neurons of the premotor cortex elicits a brisk proliferative response from neural precursor and oligodendroglial precursor cells in the deep layers of cortex and subcortical white matter, a subset of which differentiate into mature oligodendrocytes that persist weeks after the cessation of stimulation. Myelin thickness increases within the active circuit. These changes in myelin and myelin-forming cells are associated with an improvement in behavioral function that can be blocked by inhibition of oligodendrocyte differentiation and myelination. Taken together, these findings illustrate the plastic nature of myelin in the mammalian brain, raising numerous conceptual and mechanistic questions.

While the present study provides evidence that active neurons influence OPC proliferation, differentiation and myelination, the relationship between these three aspects of myelin formation may not be linear or simple. Bergles and colleagues have demonstrated that OPCs can differentiate directly into oligodendrocytes without dividing and that OPC proliferation may occur in response to the decision to differentiate by a neighboring OPC (*24*). In the present study, those OPCs that differentiate without first proliferating would not be accounted for using EdU fate mapping, and so the number of newly generated oligodendrocytes may have been underestimated. Similarly, while Richardson and colleagues have recently shown that adult-born oligodendrocytes contribute to ongoing myelin remodeling (*44*), it is not yet clear exactly how this occurs. In the present study, we cannot distinguish between the possibilities that neuronal activity results in myelination of previously unmyelinated axons, that new oligodendrocytes incorporate into existing sheaths, or that existing oligodendrocytes increase the thickness of the sheath. It is also interesting to note the difference in magnitude of the robust OPC proliferative response and new oligodendrocyte generation compared to the relatively small magnitude of change in myelin thickness (~10% change in average g-ratio), suggesting an alternative fate for some of these cells.

The paradigm used here mimics practicing a complex motor task. Would volitional, repetitive execution of a complex motor task result in the same findings? Neuroimaging studies suggest that this would be the case. A diffusion tensor imaging (DTI) study of humans before and after a six-week period of practicing a new complex visuo-motor task (juggling) revealed changes in the microstructure of subcortical white matter within a brain region active in the task (*45*). Similarly, training in a complex motor task involving one limb was correlated with DTI-based indication of more developed white matter microstructure in the corpus callosum subjacent to the correlate motor cortex, precisely in the same location we observed activity-regulated oligodendrogenesis and increased thickness of myelin sheaths (*46*). The degree of complexity, directionality or repetition necessary to elicit changes in myelin microstructure is not clear. Thus, wandering around a cage may not focally alter motor circuit myelin, but repeated episodes of a specific motor task (e.g., walking in a counterclockwise circle) may elicit a response in the

relevant neural circuit that facilitates that behavior subsequently. Conversely, would hypoactivity of a circuit result in thinner myelin? Elegant studies evaluating the effects of social isolation on myelin thickness in the medial prefrontal cortex, a region important in social function, suggest that this, too, may be the case (*47*, *48*).

It may be that neuronal activity-regulated changes in myelin-forming cells are most relevant to cortical and association fiber myelin. We observed the proliferative response in the deep layers of cortex and subcortical projections, including those in the corpus callosum projecting to the contralateral motor area, but not those in deep white matter projections down the corticospinal tract. Similarly, the aforementioned DTI study of white matter changes following training in a complex visuo-motor task revealed alterations in myelin microstructure consistent with improved myelination within the subcortical association fibers underlying the intraparietal sulcus (*45*). Regional differences may exist in the response of myelin-forming cells to neuronal activity that may reflect differences inherent in cortical OPCs compared to those found in the deep white matter; cortical OPCs have a distinct developmental origin (*34*), respond differentially to mitogens (*35*), appear to contribute uniquely to the pathogenesis of glial tumors (*49*), and may respond differentially to activity-regulated signals. Alternatively, the localization of the observed effect on OPC proliferation and differentiation may reflect proximity to the neuronal cell bodies, as OPC mitogens can be released from the neuronal soma rather than from axons (*36*). A third possibility is that specific neuronal types (e.g., callosal neurons compared to corticofugal neurons) may interact differentially with myelin-forming cells.

How would small or localized changes in myelin structure affect neural circuit function? Subtle *g*-ratio changes in the 0.6-0.8 range can result in substantial changes in conduction velocity (*40*). Neural circuit function is complex and incompletely understood, but some prominent models of cortical performance (*50*) invoke the need for activity-dependent myelination as a means of balancing conductance delay and synaptic strength parameters [see (*51*) for a recent review]. It should be noted, however, that maladaptive changes in conduction delay could conversely result in perturbation of neural function by disrupting neuronal signal synchrony.

The present study may elucidate the mechanistic role of experience in brain development, defining activity-dependent adaptive changes in myelin as a dimension along which experience modulates neural function. Adult-born oligodendrocytes contribute to myelin remodeling throughout life (*44*), sensory deprivation via social isolation results in hypomyelination of the prefrontal cortex of mice (*47*, *48*) and learning a new language (*52*) or complex motor tasks (*45*) has been shown to alter white matter structure within the relevant neural circuits in humans. These studies imply the dynamic nature of cerebral myelin throughout life and the role experience may have in modulation of the brain's infrastructure. The data presented here demonstrate that the effect of experience on myelinated fiber microstructure may result from direct effects of neuronal activity on myelin-forming cells.

The potent effects of neuronal activity on OPC proliferation, oligodendrogenesis and myelination could have broad clinical implications. When dysregulated, neuronal activity-induced OPC proliferation may play a role in glioma pathogenesis, given that OPCs are thought to be the cell of origin for multiple subtypes of high-grade glioma in both children and adults (*49*, *53*). Pediatric high-grade gliomas appear linked to epigenetic dysregulation caused by driver mutations in histone H3 that may prevent effective control of such proliferation (*54*, *55*). Conversely, precisely harnessing the myelinogenic potential of neuronal-OPC interactions could yield effective regenerative strategies in diseases of myelin.

Materials and Methods

Statistical Analysis

For total EdU counts, cell identity counts, muscle morphometry analyses, and Catwalk behavioral tests (swing speed, forepaw intensity measurements, and stride length) group mean differences were assessed using two-way analysis of variance (two-way ANOVA) with Tukey or Tukey-Kramer post-hoc tests to further examine pairwise differences. Paired, two-tailed Student's t-tests were used for analysis of mean differences between the ipsilateral and contralateral sides within the same animal in MBP intensity analyses. Unpaired, two-tailed Student's t-tests were used for analysis of mean differences between animals in electron microscopy measurements. A level of $P < 0.05$ was used to designate significant differences.

As determined before data collection, animals were excluded from analysis if optogenetic stimulation did not result in the expected ambulation behavior (for Thy1::ChR2 animals) or, in the case of behavioral analysis, if the animal did not complete four successful runs characterized by variation under 60%, lasting no more than 5 seconds, and consistent movement along the CatWalk apparatus.

Mice and Housing Conditions

Male Thy1::ChR2 (The Jackson Laboratory, line #20) mice were bred with female CD1 mice (Charles River Laboratories). All experiments were performed on animals either heterozygous for Thy1::ChR2 or wild-type littermates housed in a 12-hour light:dark cycle with ad libitum access to food and water. Animals were housed 5 per cage. Male animals were used for the behavioral analysis, and both sexes were used equally for all other studies. No animals were manipulated other t7han as reported for that experimental group, i.e. there was no history of drug exposures, surgeries or behavioral testing for the animals used other than that reported for the given experimental group. All procedures were performed in accordance with guidelines set in place by the Stanford University Institutional Care and Use Committee.

Fiber Optic Placement and in Vivo Optogenetic Stimulation

On P32-33, animals were anesthetized using 1-4% isoflurane and placed in a stereotactic apparatus. After aseptically preparing the skin, the skull was exposed using a midline incision and a dental drill with a 0.5 mm burr was used to expose the brain. A fiber optic ferrule (Doric Lenses) was placed over the premotor cortex (M2) and secured with dental cement. Ferrules were implanted at the following coordinates: –0.5 mm lateral to midline, 1.0 mm anterior to bregma, –0.6 mm from the skull in the right hemisphere [as described in (*56*)]. On P35, all freely-moving animals were connected to a 100-mW 473 nm DPSS laser system with a mono fiber patch cord, and pulses of light were administered at 20 Hz. Approximately 3.7 V at 20 Hz (50-ms pulse length; 25 ms on/25 ms off) produced an output of ~1 mW which is the minimum intensity necessary to initiate the unidirectional circling behavior of the mice. The blue light from the laser penetrates approximately 0.5 mm from the tip of the fiber optic and stimulates the apical dendrites of cortical layer V neurons expressing the ChR2 opsin. M2 layer V output neurons project to M1 motor cortex, which in turn projects down the corticospinal tract, and also project to the contralateral motor cortex via the corpus callosum. For acute (3-hour) and subacute (24-hour) time points, light was administered during a 30-minute session, with alternating 30-second light exposures and 2-minute recovery periods, and mice were sacrificed either 3 hours or 24 hours, respectively, after the start of the stimulation session. For the long-term time point (4 weeks), animals were exposed to the same alternating light exposure paradigm (30 seconds on: 2 minutes off) for 10 minutes/day for 7 days beginning at P35 or P84 and sacrificed 4 weeks after the cessation of the 7-day stimulation paradigm. For the 7-

day time point, P29 mice were stimulated according to the stimulation protocol used for the 4 week time point but were sacrificed 3 hours after the final stimulation session on day 7 at P35. For all stimulation sessions, all animals were given an i.p. injection of 5-ethynyl-2'-deoxyuridine (EdU; 40 mg/kg). In order to control for stimulation in the analysis of corpus callosum, a separate group of unstimulated mice were used. In unstimulated mice, animals underwent surgery, ferrule-fiber optic implantation and EdU injections as described above but were not exposed to 20 Hz pulses of blue light. In animals treated with histone deacetylase inhibitor, mice were given an i.p. injection of trichostatin A (TSA; Selleck Chemicals; 10 mg/kg) concurrently with EdU administration. When the ferrule is properly placed over right M2, Thy1::ChR2 animals respond with increased locomotor behavior (circling) to the left (movie S1) while WT animals have no change in behavioral output.

In order to induce seizures without circling behavior, the ferrule was placed slightly more medially in M2 (–0.25 mm lateral to midline) with no change in stimulation intensity or frequency. Animals exhibited obvious motor seizure activity (tonic-clonic movements) of approximately 10 seconds in duration; at the onset of tonic-clonic movements the stimulation was held (blue light off) and animals were allowed to recover to behavioral baseline before further stimulation within the 30-minute stimulation session. Animals had an average of 5-10 brief seizures, lasting 10-15 seconds each, during the single stimulation session and were sacrificed 3 hours later.

Perfusion and Immunohistochemistry

All animals were anesthetized with avertin and transcardially perfused with 15 mL PBS. Brains were post-fixed in 4% paraformaldehyde (PFA) overnight at 4°C prior to cryoprotection in 30% sucrose. Brains were embedded in O.C.T. (Tissue-Tek) and sectioned in the coronal plane at 40 µm using a sliding microtome (Leica, HM450). Spinal cords were dissected from the column and allowed to equilibrate in 30% sucrose. From each cord, transverse segments 3 mm in length were isolated and embedded in O.C.T., and a series of 40µm transverse sections were collected using a sliding microtome (Leica, HM450). For immunohistochemistry, sections were stained using the Click-iT EdU cell proliferation kit and protocol (Invitrogen) to expose EdU labeling followed by incubation in blocking solution (3% normal donkey serum, 0.3% Triton X-100 in TBS) at room temperature for 1 hour. Goat anti-Sox2 (1:50; R&D Systems AF2018), rabbit anti-Olig2 (1:500; Millipore AB9610), goat anti-PDGFRα (1:500; R&D Systems AF1062), rabbit anti-Iba1 (1:2000; Wako 019-19741), rat anti-CD68 (1:200; Abcam AB53444), rabbit anti-GFAP (1:500; Dako Z0334), rabbit anti-Ki67 (1:500; Abcam AB155580), rabbit anti-Caspase-3 (1:500; Cell Signaling 9662), rabbit anti-Olig1 (1:500; generous gift from Dr. Charles Stiles), rabbit anti-Histone H3K9me3 (tri-methyl K9; 1:200; Abcam AB8898), rabbit anti-Acetyl-histone H3 (1:200; Millipore 06-599), goat anti-cFos (1:300; Abcam AB87655), chicken anti-MAP2 (1:10,000; Abcam AB5392), mouse anti-CC1 (1:20; Calbiochem OP80), rabbit anti-S100ß (100ug/ml; Sigma S2644) or rat anti-MBP (1:200; Abcam AB7349) were diluted in 1% blocking solution (normal donkey serum in 0.3% Triton X-100 in TBS) and incubated overnight at 4°C with the exception of the anti-CC1 antibody for which a one week incubation was used. All antibodies have been validated in the literature and/or in Antibodypedia for use in mouse immunohistochemistry. To further validate the antibodies in our hands, we confirmed that each antibody stained in the expected cellular patterns and brain-wide distributions (e.g. nuclear Sox2 staining in the subventricular zone). For the case of cleaved caspase-3 staining, we confirmed antibody staining in ischemic brain tissue as a positive control. Secondary-only stains were performed as negative controls.

The following day, sections were rinsed 3 times in 1X TBS and incubated in secondary antibody solution (1:500) and DAPI (1:1000) in 1% blocking solution at 4°C overnight. The following secondary antibodies were used: DyLight 405 donkey anti-rabbit (Jackson ImmunoResearch), Alexa 488 donkey anti-goat (Jackson ImmunoResearch), FITC donkey anti-rabbit (Jackson ImmunoResearch), FITC donkey anti-rat (Jackson ImmunoResearch), Alexa 647 donkey anti-chicken (Jackson ImmunoResearch), Alexa 647 donkey anti-mouse (Invitrogen) or Alexa 647 donkey anti-goat (Invitrogen). The next day, sections were rinsed 3 times in TBS and mounted with Krystalon (HARLECO) mounting medium.

Confocal Imaging and Quantification

All cell counting was performed by experimenters blinded to the experimental conditions using a Zeiss LSM700 scanning confocal microscope (Carl Zeiss Inc.). For EdU stereology, all EdU-labeled cells in every 12th bilateral (ipsilateral and contralateral to fiber optic ferrule) section (or every 6th for the 4 week time point tissue) throughout the extent of M2 or the corpus callosum were counted by blinded experimenters at 200X or 400X magnification, excluding those cells in the outermost field of focus (i.e. the edge of the section) as well as those within 100 µm surrounding ferrule-induced tissue damage. The total number of EdU-labeled cells per M2 or corpus callosum was determined by multiplying the number of EdU^+ cells by 12 (or 6 for the 4 week time point). For each animal, 50-100 EdU^+ cells for M2 and 15-25 EdU^+ cells for corpus callosum were randomly chosen and assessed for double-labeling with the aforementioned primary antibodies to determine the proportion of EdU^+ cells with specific cell identities or epigenetic markers. A minimum of three animals was assessed for each marker. Cells were considered double-labeled when they co-localized within the same plane. This proportion was then multiplied by the total number of EdU-labeled cells to determine the total number of cells within each M2 hemisphere or corpus callosum for every animal with that specific cell identity. For EdU quantification in the cervical spinal cord, EdU-labeled cells were counted at 200X magnification in representative 40-µm sections within the extent of the dorsal corticospinal tract. For MBP intensity measurements, forebrain sections surrounding the site of the fiber optic ferrule were used for the analysis. Z-stack images of the M2 area, both ipsilateral and contralateral to the optogenetically-stimulated side, were acquired at 100X using a Zeiss LSM700 confocal microscope and Zen 2011 imaging software. For regional analysis of MBP expression, ImageJ software (Version 1.47) was used to quantify the average fluorescent intensity of pixels in a region drawn around the entry of M2 fibers into the horn of the corpus callosum. Comparisons of intensity were made between ipsilateral and contralateral sides within a given slice. Average values across all sections were calculated for each animal and hemisphere.

For analysis of $EdU^+/CC1^+$ cells per mm^3, estimated volume measurements for ipsilateral and contralateral M2 and corpus callosum were obtained using MBF Bioscience StereoInvestigator version 11.01.2. Bright field tile images of 1:6 series of M2 and corpus callosum were obtained at 50x using Zen Zeiss software through areas that were quantified in EdU stereology counts, which amounted to 11 total slices. The Cavalieri Estimator probe was used to analyze the tissue, and boundaries of the regions of interest were determined using published mouse anatomical guides (*57*). A random sampling grid with dimensions of 50 µm × 50 µm was overlaid. Coefficients of error (Gunderson, $m = 0$) for the regions of interest were as follows: ipsilateral M2 = 0.071; contralateral M2 = 0.067; corpus callosum = 0.1. The number of $EdU^+/CC1^+$ cells per mm^3 was determined by dividing the total number of $EdU^+/CC1^+$ cells by the estimated volume analyzed for each region.

Muscle Histology and Morphometry

Thy1::ChR2 and WT mice were anesthetized with avertin, then perfused

with 10 mL PBS followed by 10 mL 2% glutaraldehyde/4% PFA/100-mM sodium cacodylate 4 weeks following the 7-day optogenetic stimulation paradigm. Forelimbs were removed, and biceps and triceps brachii muscles were dissected out bilaterally and weighed with an analytical balance. Whole muscles were embedded in paraffin, sectioned at 5 μm, and stained with hematoxylin and eosin. Blinded morphometric analysis was performed at 400X magnification (SPOT Imaging Solutions) by obtaining the mean of the shortest diameter of all muscle fibers within a single field of view (80 ± 5 fibers), excluding damaged fibers.

Electron Microscopy

Four weeks after optogenetic stimulation (as above), Thy1::ChR2 or WT mice (untreated or treated with 10 mg/kg TSA as above) were sacrificed by transcardial perfusion with Karnovsky's fixative: 2% glutaraldehyde (EMS #16000) and 4% paraformaldehyde (EMS #15700) in 0.1M sodium cacodylate (EMS #12300), pH 7.4. Bilateral premotor cortex (M2) was resected from the brain and post-fixed in Karnovsky's fixative for at least 2 weeks. Transmission electron microscopy was performed in the region of the M2 subcortical fibers as they exit cortical layer VI and enter the corpus callosum. The samples were then post-fixed in 1% osmium tetroxide (EMS #19100) for 1 hour at room temperature, washed 3 times with ultrafiltered water, then en bloc stained for 2 hours at room temperature. Samples were then dehydrated in graded ethanols (50%, 75%, and 95%) for 15 minutes each at 4° C; the samples were then allowed to equilibrate to room temperature and were rinsed in 100% ethanol 2 times, followed by acetonitrile for 15 minutes. Samples were infiltrated with EMbed-812 resin (EMS #14120) mixed 1:1 with acetonitrile for 2 hours followed by 2:1 EMbed-812:acetonitrile for 2 hours. The samples were then placed into EMbed-812 for 2 hours, then placed into TAAB capsules filled with fresh resin, which were then placed into a 65°C oven overnight. Sections were taken between 75 and 90 nm on a Leica Ultracut S (Leica, Wetzlar, Germany) and mounted on Formvar/carbon coated slot grids (EMS #FCF2010-Cu) or 100 mesh Cu grids (EMS #FCF100-Cu). Grids were contrast stained for 30 seconds in 3.5% uranyl acetate in 50% acetone followed by staining in 0.2% lead citrate for 30 seconds. Samples were imaged using a JEOL JEM-1400 TEM at 120kV and images were collected using a Gatan Orius digital camera. With experimenters blinded to sample identity and condition, axons ipsilateral and contralateral to ferrule placement were analyzed for *g*-ratios calculated by dividing the shortest axonal diameter by the corresponding axonal-plus-sheath diameter (diameter of axon/diameter of axon + myelin sheath). For each group, 235 to 422 axons were scored. Measurements of *g*-ratio were confirmed by a second, blinded rater.

Myelinated fiber density was analyzed by quantifying the number of myelinated axons per 8000X electron micrograph. An average of 71 such images were quantified per animal and the average number of myelinated fibers per image was calculated for each animal. We did not find a significant change in the density of myelinated fibers (2.59 ± 0.65 myelinated axons per field in Thy1::ChR2 mice vs. 1.88 ± 0.47 myelinated fibers per field in WT mice on the side ipsilateral to optogenetic stimulation, $n = 4$ Thy1::ChR2 animals and 3 WT animals; $P = 0.45$). However, this analysis is complicated by the fact that the distribution of projection axons entering the corpus callosum from motor cortex is shaped like an inverted cone or a funnel in which the same number of axons would appear less dense superiorly at the base of the cone and denser inferiorly at the vertex of the cone. Thus, even micrometer changes in the level of analysis would affect the density of fibers observed. While Thy1::ChR2 and WT mice were sampled in the same way and at the same approximate level, we believe that the variability introduced by the conformation of the structure makes it difficult to detect small changes in myelinated fiber density. We thus do not detect pronounced differences, but cannot exclude small changes in myelinated fiber density following optogenetic stimulation.

Behavioral Analysis

To investigate the effect of unilateral optogenetic stimulation of the corticospinal tract on motor output, the CatWalk gait analysis system (Noldus, Netherlands) was used. The apparatus consists of a glass walkway with opaque, black siding that is internally illuminated with fluorescent lights via one of the long edges of the glass floor. As the mouse traverses the glass floor, the footprints cause the light to be reflected downward and are recorded by a camera positioned underneath the glass and relayed to an adjacent computer. For a detailed description of the CatWalk method see Hamers et al. (*41*). To ensure consistent running, mice were acclimated to handling for several weeks before recording, and all tests were run in a dark room. Only male mice were used to reduce variability in output measures between males and females based on body weight. Animals were tested 4 weeks after the cessation of the 7-day optogenetic stimulation paradigm previously described. Male mice that did not undergo surgery and optogenetic stimulation were used to control for changes in behavior due to experimental manipulation. No behavioral training on the CatWalk apparatus was performed. Behavioral testing was performed during the light cycle. Four successful runs (with success being characterized by variation under 60%, lasting no more than 5 seconds, and consistent movement) were processed with the CatWalk XT 9.0 software. A sample size calculation using the ANOVA sample size calculator in SigmaPlot was used and the numbers (the standard deviation and the minimum detectable difference in means) were based on an initial pilot study comparing untreated Thy1::ChR2 to WT animals using a power of 0.8 and an alpha of 0.05; this resulted in a sample size of 5 animals.

Our a priori hypothesis was that swing speed, as a sensitive measure of motor system function, would be selectively improved if myelination was increased within the premotor circuit. We did not expect to see a difference in stance or paw strike intensity as a result of an increase in myelination. In this study, only the following three parameters were analyzed:

Swing speed: the speed (cm/s) of the paw during limb swinging. Swing speed was calculated as the difference in speed between the left forepaw and the right forepaw; thus, a positive value signifies a faster left forepaw swing speed compared to the right forepaw.

Stride length: the distance (cm) between successive placements of the same paw. Calculation of stride length is based on the X-coordinates of the center of the paw print of two consecutive placements of the same paw during maximum contact of the paw with the glass floor.

Paw intensity: the mean intensity (0-255, arbitrary units) of the paw print as projected onto the glass floor. The intensity of a print depends on the degree of contact between a paw and the glass plate and increases with increasing pressure.

References and Notes

1. P. I. Yakovlev, "The myelogenetic cycles of regional maturation of the brain." in *Regional Development of the Brain in Early Life*, A. Minkowski, Ed. (Blackwell Scientific Publications, Oxford, 1967), pp. 3–70.
2. C. Lebel, M. Gee, R. Camicioli, M. Wieler, W. Martin, C. Beaulieu, Diffusion tensor imaging of white matter tract evolution over the lifespan. *Neuroimage* **60**, 340–352 (2012). Medline doi:10.1016/j.neuroimage.2011.11.094
3. F. M. Benes, Myelination of cortical-hippocampal relays during late adolescence. *Schizophr. Bull.* **15**, 585–593 (1989). Medline doi:10.1093/schbul/15.4.585
4. E. Zuccaro, P. Arlotta, The quest for myelin in the adult brain. *Nat. Cell Biol.* **15**, 572–575 (2013). Medline doi:10.1038/ncb2750
5. B. A. Barres, M. C. Raff, Proliferation of oligodendrocyte precursor cells depends on electrical activity in axons. *Nature* **361**, 258–260 (1993). Medline doi:10.1038/361258a0
6. C. Demerens, B. Stankoff, M. Logak, P. Anglade, B. Allinquant, F. Couraud,

B. Zalc, C. Lubetzki, Induction of myelination in the central nervous system by electrical activity. *Proc. Natl. Acad. Sci. U.S.A.* **93**, 9887–9892 (1996). Medline doi:10.1073/pnas.93.18.9887
7. B. Stevens, S. Tanner, R. D. Fields, Control of myelination by specific patterns of neural impulses. *J. Neurosci.* **18**, 9303–9311 (1998). Medline
8. T. Ishibashi, K. A. Dakin, B. Stevens, P. R. Lee, S. V. Kozlov, C. L. Stewart, R. D. Fields, Astrocytes promote myelination in response to electrical impulses. *Neuron* **49**, 823–832 (2006). Medline doi:10.1016/j.neuron.2006.02.006
9. H. Wake, P. R. Lee, R. D. Fields, Control of local protein synthesis and initial events in myelination by action potentials. *Science* **333**, 1647–1651 (2011).doi:10.1126/science.1206998
10. Q. Li, M. Brus-Ramer, J. H. Martin, J. W. McDonald, Electrical stimulation of the medullary pyramid promotes proliferation and differentiation of oligodendrocyte progenitor cells in the corticospinal tract of the adult rat. *Neurosci. Lett.* **479**, 128–133 (2010). Medline doi:10.1016/j.neulet.2010.05.043
11. G. Goldsberry, D. Mitra, D. MacDonald, Z. Patay, Accelerated myelination with motor system involvement in a neonate with immediate postnatal onset of seizures and hemimegalencephaly. *Epilepsy Behav.* **22**, 391–394 (2011). Medline doi:10.1016/j.yebeh.2011.06.025
12. D. E. Bergles, J. D. Roberts, P. Somogyi, C. E. Jahr, Glutamatergic synapses on oligodendrocyte precursor cells in the hippocampus. *Nature* **405**, 187–191 (2000). Medline doi:10.1038/35012083
13. S. C. Lin, J. H. Huck, J. D. Roberts, W. B. Macklin, P. Somogyi, D. E. Bergles, Climbing fiber innervation of NG2-expressing glia in the mammalian cerebellum. *Neuron* **46**, 773–785 (2005). Medline doi:10.1016/j.neuron.2005.04.025
14. R. Káradóttir, P. Cavelier, L. H. Bergersen, D. Attwell, NMDA receptors are expressed in oligodendrocytes and activated in ischaemia. *Nature* **438**, 1162–1166 (2005). Medline doi:10.1038/nature04302
15. J. L. Ziskin, A. Nishiyama, M. Rubio, M. Fukaya, D. E. Bergles, Vesicular release of glutamate from unmyelinated axons in white matter. *Nat. Neurosci.* **10**, 321–330 (2007). Medline doi:10.1038/nn1854
16. J. M. Mangin, A. Kunze, R. Chittajallu, V. Gallo, Satellite NG2 progenitor cells share common glutamatergic inputs with associated interneurons in the mouse dentate gyrus. *J. Neurosci.* **28**, 7610–7623 (2008). Medline doi:10.1523/JNEUROSCI.1355-08.2008
17. L. M. De Biase, A. Nishiyama, D. E. Bergles, Excitability and synaptic communication within the oligodendrocyte lineage. *J. Neurosci.* **30**, 3600–3611 (2010). Medline doi:10.1523/JNEUROSCI.6000-09.2010
18. L. M. De Biase, S. H. Kang, E. G. Baxi, M. Fukaya, M. L. Pucak, M. Mishina, P. A. Calabresi, D. E. Bergles, NMDA receptor signaling in oligodendrocyte progenitors is not required for oligodendrogenesis and myelination. *J. Neurosci.* **31**, 12650–12662 (2011). Medline doi:10.1523/JNEUROSCI.2455-11.2011
19. B. R. Arenkiel, J. Peca, I. G. Davison, C. Feliciano, K. Deisseroth, G. J. Augustine, M. D. Ehlers, G. Feng, In vivo light-induced activation of neural circuitry in transgenic mice expressing channelrhodopsin-2. *Neuron* **54**, 205–218 (2007). Medline doi:10.1016/j.neuron.2007.03.005
20. H. Wang, J. Peca, M. Matsuzaki, K. Matsuzaki, J. Noguchi, L. Qiu, D. Wang, F. Zhang, E. Boyden, K. Deisseroth, H. Kasai, W. C. Hall, G. Feng, G. J. Augustine, High-speed mapping of synaptic connectivity using photostimulation in Channelrhodopsin-2 transgenic mice. *Proc. Natl. Acad. Sci. U.S.A.* **104**, 8143–8148 (2007). Medline doi:10.1073/pnas.0700384104
21. E. S. Boyden, F. Zhang, E. Bamberg, G. Nagel, K. Deisseroth, Millisecond-timescale, genetically targeted optical control of neural activity. *Nat. Neurosci.* **8**, 1263–1268 (2005). Medline doi:10.1038/nn1525
22. O. Yizhar, L. E. Fenno, T. J. Davidson, M. Mogri, K. Deisseroth, Optogenetics in neural systems. *Neuron* **71**, 9–34 (2011). Medline doi:10.1016/j.neuron.2011.06.004
23. C. M. Gremel, R. M. Costa, Premotor cortex is critical for goal-directed actions. *Front. Comput. Neurosci.* **7**, 110 (2013). Medline doi:10.3389/fncom.2013.00110
24. E. G. Hughes, S. H. Kang, M. Fukaya, D. E. Bergles, Oligodendrocyte progenitors balance growth with self-repulsion to achieve homeostasis in the adult brain. *Nat. Neurosci.* **16**, 668–676 (2013). Medline doi:10.1038/nn.3390
25. V. E. Miron, A. Boyd, J. W. Zhao, T. J. Yuen, J. M. Ruckh, J. L. Shadrach, P. van Wijngaarden, A. J. Wagers, A. Williams, R. J. Franklin, C. ffrench-Constant, M2 microglia and macrophages drive oligodendrocyte differentiation during CNS remyelination. *Nat. Neurosci.* **16**, 1211–1218 (2013). Medline doi:10.1038/nn.3469
26. C. Y. Brazel, T. L. Limke, J. K. Osborne, T. Miura, J. Cai, L. Pevny, M. S. Rao, Sox2 expression defines a heterogeneous population of neurosphere-forming cells in the adult murine brain. *Aging Cell* **4**, 197–207 (2005). Medline doi:10.1111/j.1474-9726.2005.00158.x
27. M. L. Monje, H. Toda, T. D. Palmer, Inflammatory blockade restores adult hippocampal neurogenesis. *Science* **302**, 1760–1765 (2003). doi:10.1126/science.1088417
28. C. T. Ekdahl, J. H. Claasen, S. Bonde, Z. Kokaia, O. Lindvall, Inflammation is detrimental for neurogenesis in adult brain. *Proc. Natl. Acad. Sci. U.S.A.* **100**, 13632–13637 (2003). Medline doi:10.1073/pnas.2234031100
29. O. Butovsky, Y. Ziv, A. Schwartz, G. Landa, A. E. Talpalar, S. Pluchino, G. Martino, M. Schwartz, Microglia activated by IL-4 or IFN-γ differentially induce neurogenesis and oligodendrogenesis from adult stem/progenitor cells. *Mol. Cell. Neurosci.* **31**, 149–160 (2006). Medline doi:10.1016/j.mcn.2005.10.006
30. Y. Imai, I. Ibata, D. Ito, K. Ohsawa, S. Kohsaka, A novel gene iba1 in the major histocompatibility complex class III region encoding an EF hand protein expressed in a monocytic lineage. *Biochem. Biophys. Res. Commun.* **224**, 855–862 (1996). Medline doi:10.1006/bbrc.1996.1112
31. D. Ito, Y. Imai, K. Ohsawa, K. Nakajima, Y. Fukuuchi, S. Kohsaka, Microglia-specific localisation of a novel calcium binding protein, Iba1. *Brain Res. Mol. Brain Res.* **57**, 1–9 (1998). Medline doi:10.1016/S0169-328X(98)00040-0
32. M. B. Graeber, W. J. Streit, R. Kiefer, S. W. Schoen, G. W. Kreutzberg, New expression of myelomonocytic antigens by microglia and perivascular cells following lethal motor neuron injury. *J. Neuroimmunol.* **27**, 121–132 (1990). Medline doi:10.1016/0165-5728(90)90061-Q
33. P. J. Kingham, M. L. Cuzner, J. M. Pocock, Apoptotic pathways mobilized in microglia and neurones as a consequence of chromogranin A-induced microglial activation. *J. Neurochem.* **73**, 538–547 (1999). Medline doi:10.1046/j.1471-4159.1999.0730538.x
34. T. Yue, K. Xian, E. Hurlock, M. Xin, S. G. Kernie, L. F. Parada, Q. R. Lu, A critical role for dorsal progenitors in cortical myelination. *J. Neurosci.* **26**, 1275–1280 (2006). Medline doi:10.1523/JNEUROSCI.4717-05.2006
35. R. A. Hill, K. D. Patel, J. Medved, A. M. Reiss, A. Nishiyama, NG2 cells in white matter but not gray matter proliferate in response to PDGF. *J. Neurosci.* **33**, 14558–14566 (2013). Medline doi:10.1523/JNEUROSCI.2001-12.2013
36. M. Fruttiger, A. R. Calver, W. D. Richardson, Platelet-derived growth factor is constitutively secreted from neuronal cell bodies but not from axons. *Curr. Biol.* **10**, 1283–1286 (2000). Medline doi:10.1016/S0960-9822(00)00757-0
37. S. Shen, J. Li, P. Casaccia-Bonnefil, Histone modifications affect timing of oligodendrocyte progenitor differentiation in the developing rat brain. *J. Cell Biol.* **169**, 577–589 (2005). Medline doi:10.1083/jcb.200412101
38. M. Wu, M. Hernandez, S. Shen, J. K. Sabo, D. Kelkar, J. Wang, R. O'Leary, G. R. Phillips, H. S. Cate, P. Casaccia, Differential modulation of the oligodendrocyte transcriptome by sonic hedgehog and bone morphogenetic protein 4 via opposing effects on histone acetylation. *J. Neurosci.* **32**, 6651–6664 (2012). Medline doi:10.1523/JNEUROSCI.4876-11.2012
39. H. A. Arnett, S. P. Fancy, J. A. Alberta, C. Zhao, S. R. Plant, S. Kaing, C. S. Raine, D. H. Rowitch, R. J. Franklin, C. D. Stiles, bHLH transcription factor Olig1 is required to repair demyelinated lesions in the CNS. *Science* **306**, 2111–2115 (2004). doi:10.1126/science.1103709
40. R. S. Smith, Z. J. Koles, Myelinated nerve fibers: Computed effect of myelin thickness on conduction velocity. *Am. J. Physiol.* **219**, 1256–1258 (1970). Medline
41. F. P. Hamers, A. J. Lankhorst, T. J. van Laar, W. B. Veldhuis, W. H. Gispen, Automated quantitative gait analysis during overground locomotion in the rat: Its application to spinal cord contusion and transection injuries. *J. Neurotrauma* **18**, 187–201 (2001). Medline doi:10.1089/08977150150502613
42. P. Shi, M. A. Scott, B. Ghosh, D. Wan, Z. Wissner-Gross, R. Mazitschek, S. J. Haggarty, M. F. Yanik, Synapse microarray identification of small molecules that enhance synaptogenesis. *Nat. Commun.* **2**, 510 (2011). Medline doi:10.1038/ncomms1518
43. M. J. Morris, M. Mahgoub, E. S. Na, H. Pranav, L. M. Monteggia, Loss of histone deacetylase 2 improves working memory and accelerates extinction learning. *J. Neurosci.* **33**, 6401–6411 (2013). Medline

doi:10.1523/JNEUROSCI.1001-12.2013
44. K. M. Young, K. Psachoulia, R. B. Tripathi, S. J. Dunn, L. Cossell, D. Attwell, K. Tohyama, W. D. Richardson, Oligodendrocyte dynamics in the healthy adult CNS: Evidence for myelin remodeling. *Neuron* **77**, 873–885 (2013). Medline doi:10.1016/j.neuron.2013.01.006
45. J. Scholz, M. C. Klein, T. E. Behrens, H. Johansen-Berg, Training induces changes in white-matter architecture. *Nat. Neurosci.* **12**, 1370–1371 (2009). Medline doi:10.1038/nn.2412
46. C. Sampaio-Baptista, A. A. Khrapitchev, S. Foxley, T. Schlagheck, J. Scholz, S. Jbabdi, G. C. DeLuca, K. L. Miller, A. Taylor, N. Thomas, J. Kleim, N. R. Sibson, D. Bannerman, H. Johansen-Berg, Motor skill learning induces changes in white matter microstructure and myelination. *J. Neurosci.* **33**, 19499–19503 (2013). Medline doi:10.1523/JNEUROSCI.3048-13.2013
47. J. Liu, K. Dietz, J. M. DeLoyht, X. Pedre, D. Kelkar, J. Kaur, V. Vialou, M. K. Lobo, D. M. Dietz, E. J. Nestler, J. Dupree, P. Casaccia, Impaired adult myelination in the prefrontal cortex of socially isolated mice. *Nat. Neurosci.* **15**, 1621–1623 (2012). Medline doi:10.1038/nn.3263
48. M. Makinodan, K. M. Rosen, S. Ito, G. Corfas, A critical period for social experience-dependent oligodendrocyte maturation and myelination. *Science* **337**, 1357–1360 (2012).doi:10.1126/science.1220845
49. C. Liu, J. C. Sage, M. R. Miller, R. G. Verhaak, S. Hippenmeyer, H. Vogel, O. Foreman, R. T. Bronson, A. Nishiyama, L. Luo, H. Zong, Mosaic analysis with double markers reveals tumor cell of origin in glioma. *Cell* **146**, 209–221 (2011). Medline doi:10.1016/j.cell.2011.06.014
50. P. R. Roelfsema, A. K. Engel, P. König, W. Singer, Visuomotor integration is associated with zero time-lag synchronization among cortical areas. *Nature* **385**, 157–161 (1997). Medline doi:10.1038/385157a0
51. S. Pajevic, P. J. Basser, R. D. Fields, Role of myelin plasticity in oscillations and synchrony of neuronal activity. *Neuroscience* (2013). Medline doi:10.1016/j.neuroscience.2013.11.007
52. A. A. Schlegel, J. J. Rudelson, P. U. Tse, White matter structure changes as adults learn a second language. *J. Cogn. Neurosci.* **24**, 1664–1670 (2012). Medline doi:10.1162/jocn_a_00240
53. M. Monje, S. S. Mitra, M. E. Freret, T. B. Raveh, J. Kim, M. Masek, J. L. Attema, G. Li, T. Haddix, M. S. Edwards, P. G. Fisher, I. L. Weissman, D. H. Rowitch, H. Vogel, A. J. Wong, P. A. Beachy, Hedgehog-responsive candidate cell of origin for diffuse intrinsic pontine glioma. *Proc. Natl. Acad. Sci. U.S.A.* **108**, 4453–4458 (2011). Medline doi:10.1073/pnas.1101657108
54. G. Wu, A. Broniscer, T. A. McEachron, C. Lu, B. S. Paugh, J. Becksfort, C. Qu, L. Ding, R. Huether, M. Parker, J. Zhang, A. Gajjar, M. A. Dyer, C. G. Mullighan, R. J. Gilbertson, E. R. Mardis, R. K. Wilson, J. R. Downing, D. W. Ellison, J. Zhang, S. J. Baker; St. Jude Children's Research Hospital–Washington University Pediatric Cancer Genome Project, Somatic histone H3 alterations in pediatric diffuse intrinsic pontine gliomas and non-brainstem glioblastomas. *Nat. Genet.* **44**, 251–253 (2012). Medline doi:10.1038/ng.1102
55. J. Schwartzentruber, A. Korshunov, X. Y. Liu, D. T. Jones, E. Pfaff, K. Jacob, D. Sturm, A. M. Fontebasso, D. A. Quang, M. Tönjes, V. Hovestadt, S. Albrecht, M. Kool, A. Nantel, C. Konermann, A. Lindroth, N. Jäger, T. Rausch, M. Ryzhova, J. O. Korbel, T. Hielscher, P. Hauser, M. Garami, A. Klekner, L. Bognar, M. Ebinger, M. U. Schuhmann, W. Scheurlen, A. Pekrun, M. C. Frühwald, W. Roggendorf, C. Kramm, M. Dürken, J. Atkinson, P. Lepage, A. Montpetit, M. Zakrzewska, K. Zakrzewski, P. P. Liberski, Z. Dong, P. Siegel, A. E. Kulozik, M. Zapatka, A. Guha, D. Malkin, J. Felsberg, G. Reifenberger, A. von Deimling, K. Ichimura, V. P. Collins, H. Witt, T. Milde, O. Witt, C. Zhang, P. Castelo-Branco, P. Lichter, D. Faury, U. Tabori, C. Plass, J. Majewski, S. M. Pfister, N. Jabado, Driver mutations in histone H3.3 and chromatin remodelling genes in paediatric glioblastoma. *Nature* **482**, 226–231 (2012). Medline doi:10.1038/nature10833
56. F. Zhang, V. Gradinaru, A. R. Adamantidis, R. Durand, R. D. Airan, L. de Lecea, K. Deisseroth, Optogenetic interrogation of neural circuits: Technology for probing mammalian brain structures. *Nat. Protoc.* **5**, 439–456 (2010). Medline doi:10.1038/nprot.2009.226
57. B. J. Franklin, G. Paxinos, *The Mouse Brain* (Elsevier, New York, 2008).
58. J. D. Cahoy, B. Emery, A. Kaushal, L. C. Foo, J. L. Zamanian, K. S. Christopherson, Y. Xing, J. L. Lubischer, P. A. Krieg, S. A. Krupenko, W. J. Thompson, B. A. Barres, A transcriptome database for astrocytes, neurons, and oligodendrocytes: A new resource for understanding brain development and function. *J. Neurosci.* **28**, 264–278 (2008). Medline doi:10.1523/JNEUROSCI.4178-07.2008

Acknowledgments: The authors gratefully acknowledge support from the National Institute of Neurological Disorders and Stroke (NINDS K08NS070926 to M.M.; R01 EY10257 to B.A.B.), California Institute for Regenerative Medicine (CIRM RB4-06093 and RN3-06510 to M.M.), Alex's Lemonade Stand Foundation (M.M.), McKenna Claire Foundation (M.M.), The Cure Starts Now (M.M.), Lyla Nsouli Foundation (M.M.), the Dylan Jewett, Connor Johnson, Zoey Ganesh, Dylan Frick, Abigail Jensen, Wayland Villars, and Jennifer Kranz Memorial Funds (M.M.), Ludwig Foundation (M.M.), Price Family Charitable Fund (M.M.) Stanford Medical Scientist Training Program (D.P., C.M., G.L.L.), Stanford Institute for Neuro-Innovation and Translational Neurosciences (M.M.), the Child Health Research Institute (M.M. and E.M.G.), Lucile Packard Foundation for Children's Health, Stanford CTSA (UL1 RR025744 to E.M.G.), Howard Hughes Medical Institute Fellowship of the Life Sciences Research Foundation (J.B.Z.), and the Bezos Family Foundation (I.I.), Child Health Research Institute at Stanford Anne T. and Robert M. Bass Endowed Faculty Scholarship in Pediatric Cancer and Blood Diseases (M.M.). Special thanks to J. Perrino of the Electron Microscopy Core of the Stanford University Cell Sciences Imaging Facility for technical support with transmission electron microscopy, to S. Chen for the illustration accompanying the print summary of this work, and to J. Lennon, K. Lechtenberg, H. Venkatesh and M. E. Freret for critical reading of the manuscript.

Supplementary Materials
www.sciencemag.org/cgi/content/full/science.1252304/DC1
Figs. S1 to S10
Reference (*58*)
Movie S1

17 February 2014; accepted 28 March 2014
Published online 10 April 2014
10.1126/science.1252304

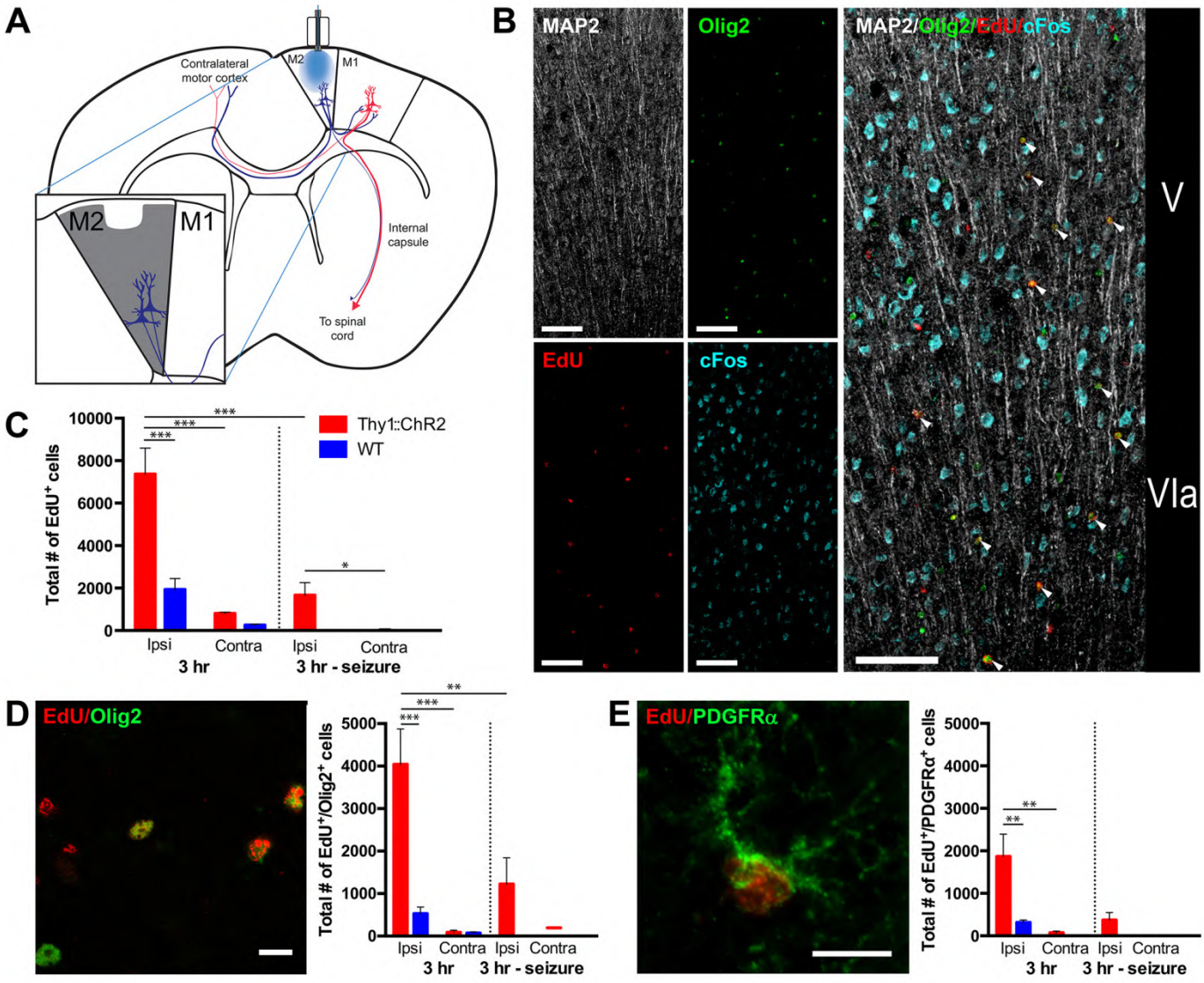

Fig. 1. Neuronal activity that elicits complex motor behavior stimulates OPC proliferation in premotor cortex. (**A**) Schematic of optogenetic stimulation with simplified M2 circuit projections; expanded view shows area quantified. (**B**) Proliferating oligodendroglial lineage cells are found near active neuronal cell bodies in the deep layers of the optogenetically stimulated M2 motor cortex. Confocal micrograph (split view on the left; composite image on the right) of the M2 deep cortical layers V and VIa three hours following optogenetic stimulation in a Thy1::ChR2 mouse. The immediate early gene c-Fos (cyan) indicates recent neuronal activity. MAP2 (white) indicates neuronal cell bodies and apical dendrites. Proliferating cells marked by EdU (red) are seen throughout the deep cortical layers and frequently co-localize with the oligodendroglial lineage marker Olig2 (green; co-localized $EdU^+/Olig2^+$ cells are indicated by the white arrowheads.) Scale bar = 100 μm. (**C**) Total EdU^+ cells in M2 of P35 (*n* = 3/group) mice three hours following optogenetic stimulation; the M2 regions ipsilateral and contralateral to the site of the optical fiber are quantified. (**D**) Representative confocal micrograph (200X) of EdU^+ cells (red) and $Olig2^+$ (green) together with total number of $EdU^+/Olig2^+$ cells in M2 three hours following optogenetic manipulation. (**E**) Representative confocal micrograph (400X) of an EdU-marked (red) PDGFRα$^+$ (green) OPC, together with total number of EdU-marked OPCs in M2 three hours following optogenetic manipulation. In all graphs, red bars = Thy1::ChR2 mice and blue bars = WT littermate controls identically

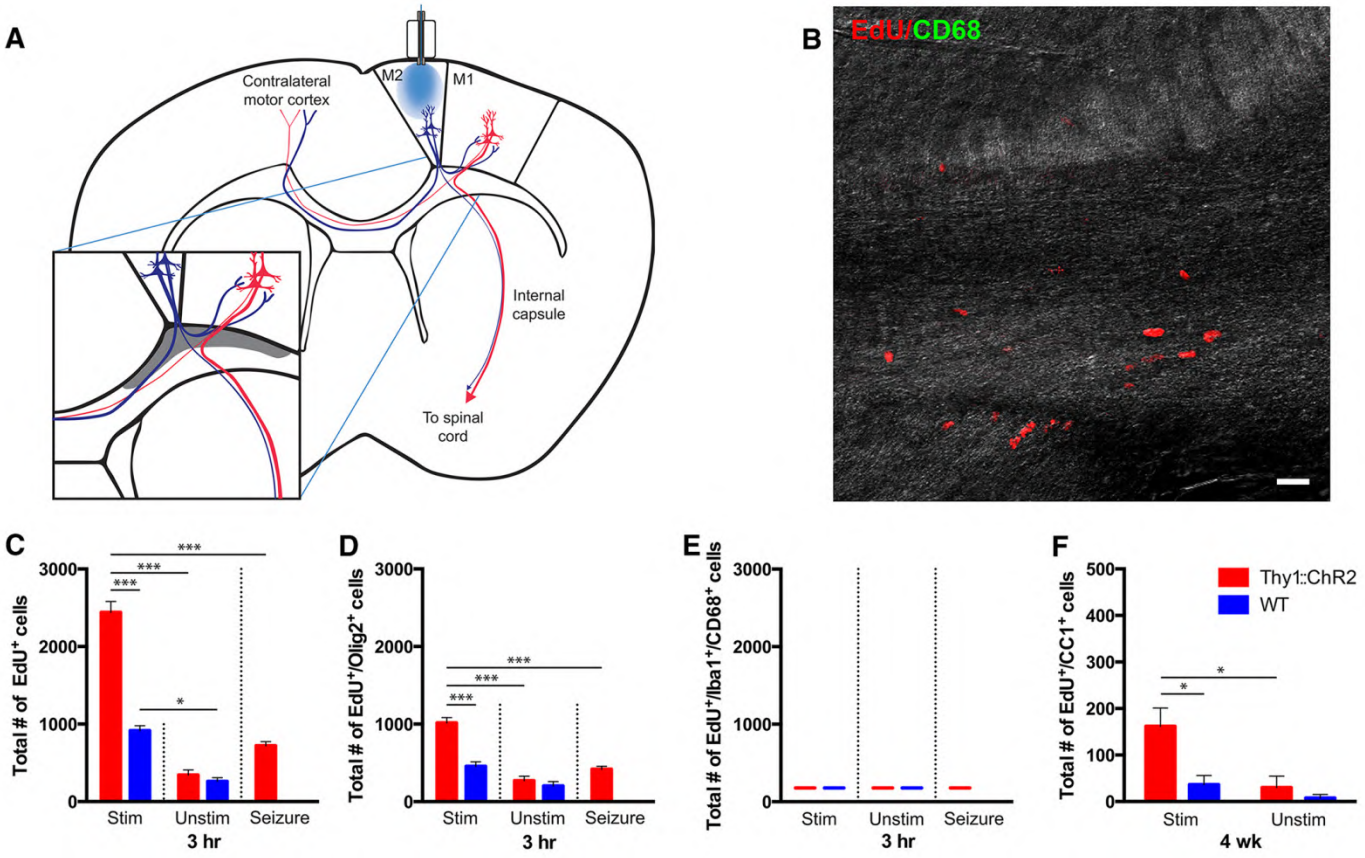

Fig. 2. Oligodendroglial lineage cells in corpus callosum respond to premotor circuit activity. (**A**) Schematic of optogenetic stimulation with simplified M2 circuit projections; expanded view shows area quantified in corpus callosum (shaded gray). (**B**) Confocal micrograph from a stimulated Thy1::ChR2 corpus callosum overlaid on a DIC background to illustrate regional tissue architecture. Activated microglial marker CD68 = green, EdU = red. No EdU^+ activated microglia were detected in the corpus callosum of stimulated or unstimulated mice. Scale bar = 20 μm. (**C** to **E**) Total EdU^+ (C), $EdU^+/Olig2^+$ (D) and $EdU/Iba1^+/CD68^+$ cells (E) in the indicated region of corpus callosum of P35 stimulated (*n* = 3/group) or unstimulated (*n* = 3/group) mice three hours following optogenetic stimulation. (**F**) Total number of $EdU^+/CC1^+$ mature oligodendrocytes 4 weeks following premotor cortex optogenetic stimulation (or no stimulation) at P35 in Thy1::ChR2 (*n* = 4/group) or WT (*n* = 3/group) mice. In all graphs, red bars = Thy1::ChR2 mice and blue bars = WT littermate controls identically manipulated. As the corpus callosum is a single structure, the contralateral structure does not serve as an internal control for stimulation. Thus, an unstimulated group ("unstim") was included in corpus callosum analyses in which surgery was performed and the optical-neural interface was placed but no light exposure occurred. Mice in whom seizures were induced rather than ambulatory behavior are shown on the right hand side of the graph (*n* = 3/group). $*P < 0.05$, $**P < 0.01$, $***P < 0.001$. Error bars, SEM.

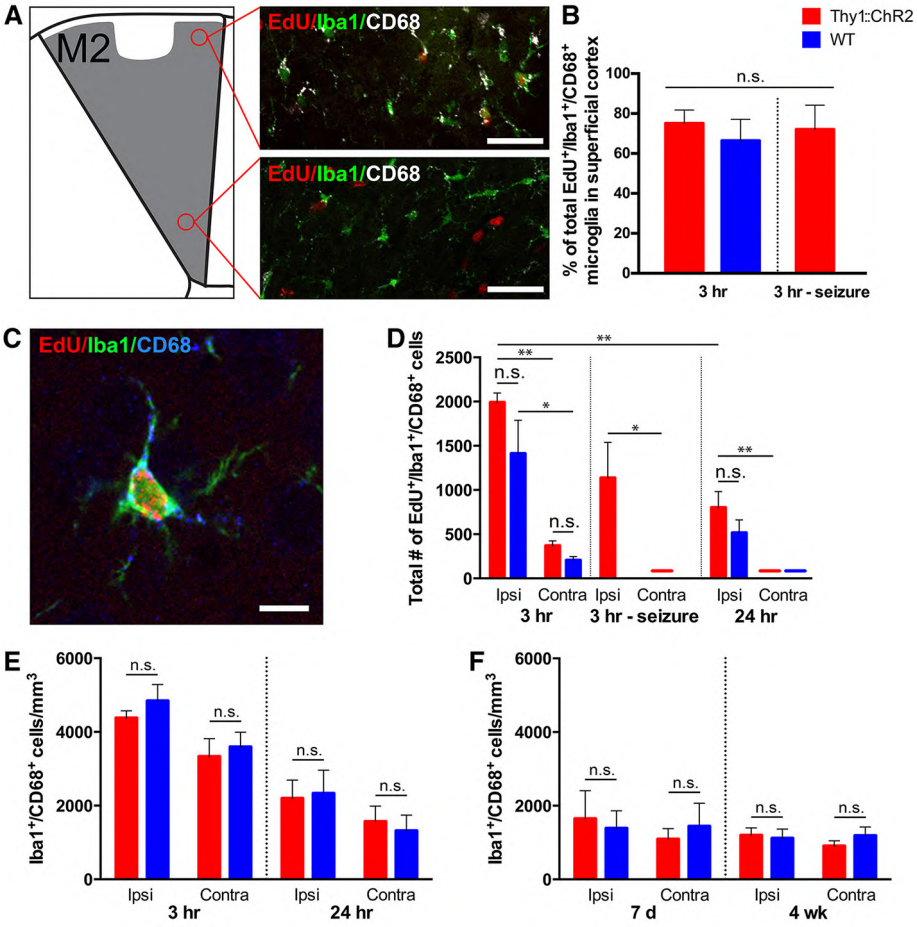

Fig. 3. Microglial inflammatory response to optical fiber manipulation is equivalent in Thy1::ChR2 and WT mice. (**A**) The majority of reactive microglia are localized to superficial cortex (layer I), near the site of the optical fiber placement. Representative confocal micrographs illustrating CD68$^+$ activated microglia in the superficial M2 cortex in comparison to largely CD68$^-$ microglia in deep cortex (layer V/VI). EdU = red, pan-microglial marker Iba1 = green, activated microglial marker CD68 = white. Scale bar = 50 µm. (**B**) Percentage of EdU-marked activated microglia (Iba1$^+$/CD68$^+$) in superficial versus deep layers of M2 cortex ipsilateral to the optical fiber, three hours following blue light stimulation in Thy1::ChR2 and WT littermate control mice. (**C**) Representative confocal micrograph illustrating a CD68$^+$ activated microglia marked with EdU. EdU = red, Iba1 = green, CD68 = blue. Scale bar = 10 µm. (**D**) Total numbers of EdU-marked activated microglia throughout M2 cortex in Thy1::ChR2 and WT littermate control mice three hours and 24 hours following optogenetic manipulation ipsilateral and contralateral to the optical fiber placement. (**E**) Density of total CD68$^+$ microglia throughout M2 cortex ipsilateral and contralateral to the optical fiber placement at three hours and 24 hours following a single 30 min session of optogenetic manipulation in P35 Thy1::ChR2 and WT mice. (**F**) Density of total CD68$^+$ microglia throughout M2 cortex ipsilateral and contralateral to the optical fiber placement following a 7-day stimulation paradigm (10 min per day for 7 days) was measured on day 7 (following stimulation from P29 – P35) or measured 4 weeks after the completion of stimulation (from P35 – P42) in Thy1::ChR2 and WT mice. In all graphs, red bars = Thy1::ChR2 mice and blue bars = WT littermate controls identically manipulated. Mice in whom seizures were induced rather than ambulatory behavior are shown to the right of the 3-hour graphs (n = 3/group). n.s. indicates $P > 0.05$. *$P < 0.05$, **$P < 0.01$, ***$P < 0.001$. Error bars, SEM.

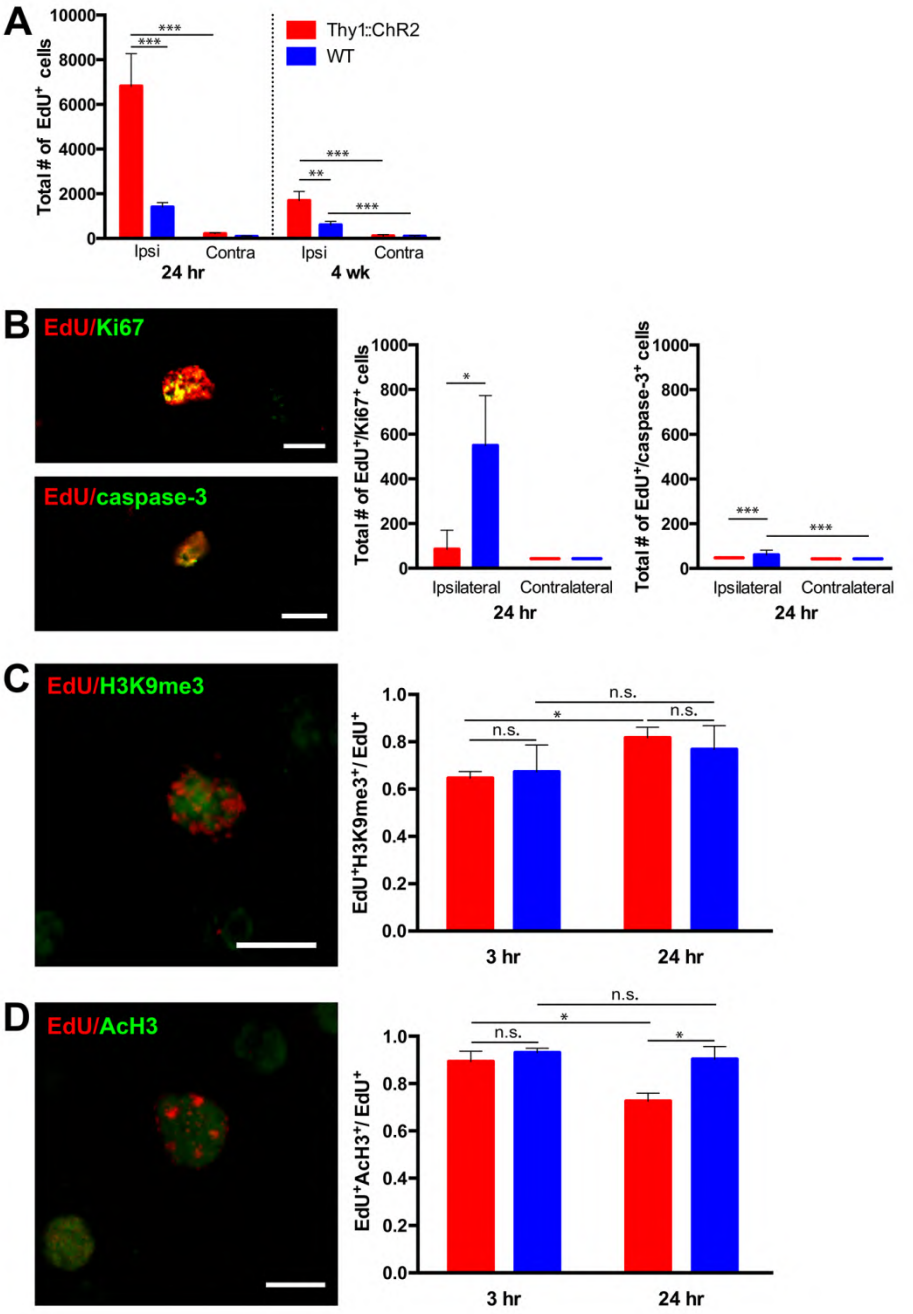

Fig. 4. Neuronal activity initiates differentiation. (**A**) Total number of EdU$^+$ cells in Thy1::ChR2 and WT mice at 24 hours (n = 4/group) and 4 weeks (n = 7/group) post-stimulation. (**B** to **D**) Representative confocal micrographs (400X) illustrating co-localization of EdU (red) with markers (green) of cell mitosis (Ki67), apoptosis (cleaved caspase-3) or histone modification markers histone H3 lysine 9 trimethylation (H3K9me3) and histone H3 acetylation (AcH3). In all graphs, red bars = Thy1::ChR2 mice and blue bars = WT littermate controls identically manipulated. *P < 0.05, **P < 0.01,***P < 0.001. n.s. indicates P > 0.05. Error bars, SEM. Scale bar = 10 μm. Value of (—) over x-axis = 0 ± 0.

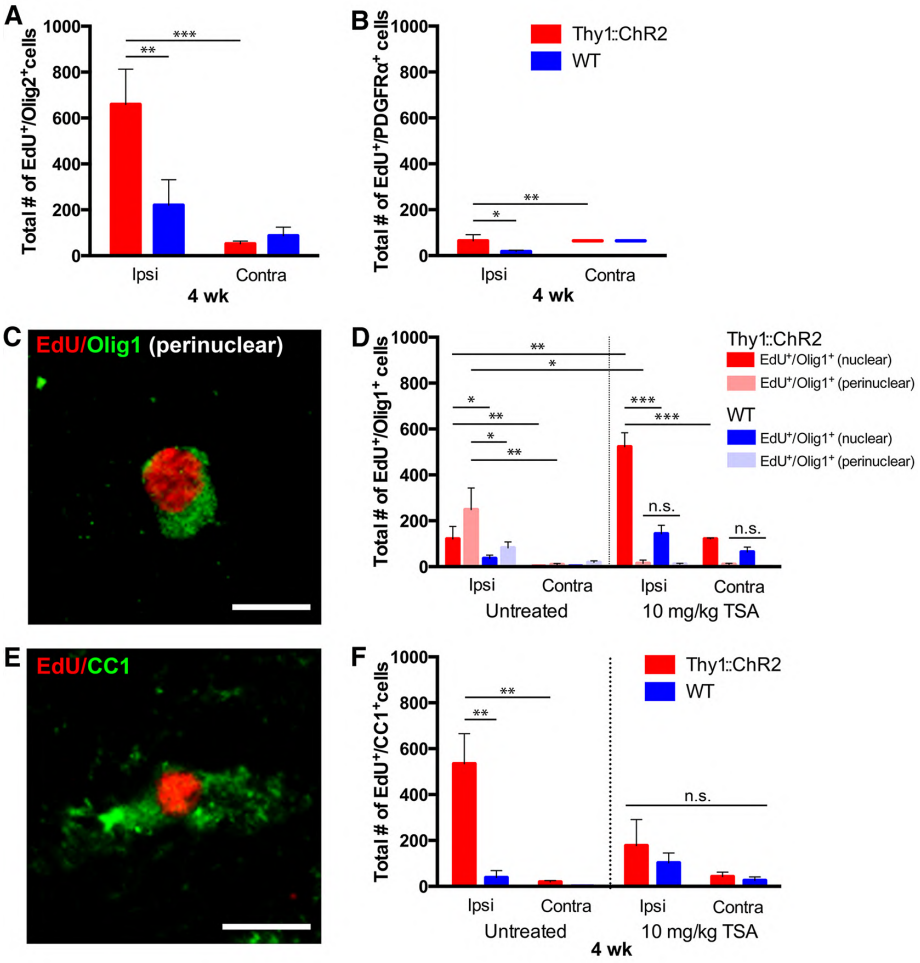

Fig. 5. Neuronal activity promotes oligodendrogenesis. Thy1::ChR2 and WT optogenetically-stimulated mice sacrificed 4 weeks following a 7-day stimulation paradigm (P35-P42) with (*n* = 4 Thy1::ChR2 and 3 WT) or without (*n* = 7/group) exposure to TSA (10 mg/kg). (**A** to **F**) Cell identity markers of EdU-marked surviving cells quantified in M2 cortex reveal that the majority of the remaining EdU$^+$ cells are in the oligodendroglial lineage [Olig2$^+$, (A)], with diminution of the oligodendrocyte precursor cell (PDGFRα$^+$) population (B) and concomitant appearance of EdU$^+$ immature oligodendrocytes [(D); nuclear Olig1$^+$; red and blue bars] and mature oligodendrocytes marked by perinuclear Olig1$^+$ [(C and D), pink and light blue bars] and CC1 (E and F). (C and E) Representative confocal micrographs (400X) illustrating co-localization of EdU (red) with perinuclear Olig1 [green; (C)] or CC1 [green; (E)]. Scale bar = 10 μm. (D and F) Administration of the histone deacetylase inhibitor trichostatin A (TSA) during the week of optogenetic stimulation results in a blockade of mature oligodendrogenesis. TSA-treated groups shown on right half of graph. Increased numbers of immature (Olig1$^{nuclear+}$) oligodendrocytes in the TSA group are consistent with an epigenetic blockade of precursor differentiation. In all graphs, red or pink bars = Thy1::ChR2 mice and blue bars = WT littermate controls identically manipulated. **P* < 0.05, ***P* < 0.01,****P* < 0.001. n.s. indicates *P* > 0.05. Error bars, SEM. Scale bar = 10 μm. Value of (—) over x-axis = 0 ± 0.

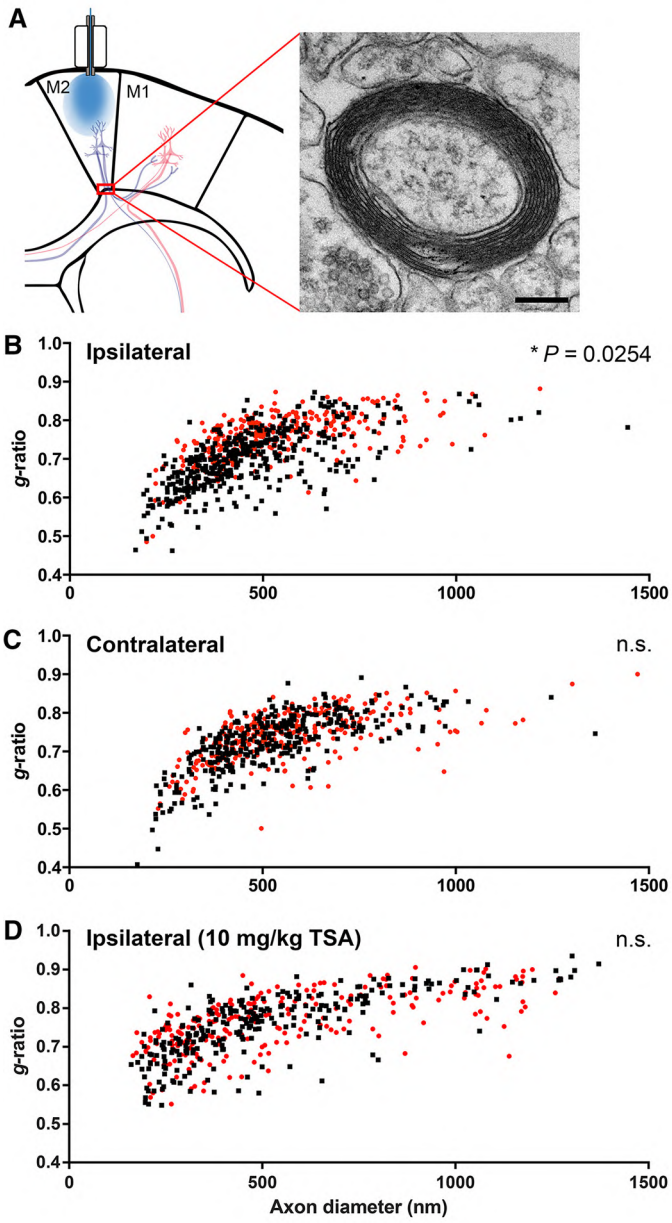

Fig. 6. Neuronal activity increases myelin thickness. (**A**) Transmission electron microscopy (TEM) was performed in the projections from premotor cortex entering corpus callosum at the level indicated (red box). A representative image demonstrating M2 deep cortical/subcortical fibers ipsilateral to optogenetic stimulation (8000X, scale bar = 200 nm). (**B** to **D**) Scatter plots of *g*-ratio as a function of axon caliber in the cortical/subcortical projections from the ipsilateral (B) and contralateral (C) M2 in Thy1::ChR2 (*n* = 4 mice) and WT (*n* = 3 mice). Black squares = Thy1::ChR2; red circles = WT. (D) Scatter plot of *g*-ratios in TSA-treated Thy1::ChR2 (black squares; *n* = 3 mice) and WT (red circles; *n* = 3 mice) ipsilateral to stimulation. **P* < 0.05, ***P* < 0.01,****P* < 0.001. n.s. indicates *P* > 0.05. Error bars, SEM.

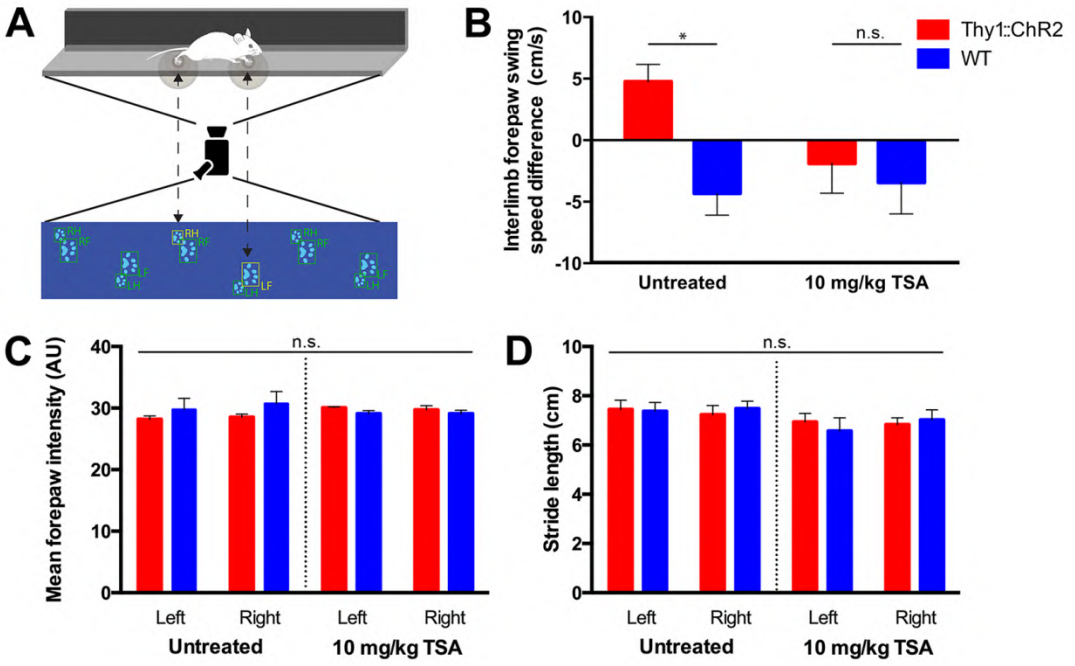

Fig. 7. Activity-regulated oligodendrogenesis and myelin remodeling correlate with improved behavioral function. CatWalk gait analysis was used to evaluate motor performance during normal gait at four weeks following the stimulation paradigm described above. (**A**) Schematic of the CatWalk apparatus is shown. Experimental mice walk through a long, narrow corridor on a touch-sensitive glass platform, under which a digital camera records paw print contours, allowing for software-guided reconstruction and analysis of gait. LF = left forepaw; LH = left hindpaw; RF = right forepaw; RH = right hindpaw. (**B**) Inter-limb forelimb swing speed (cm/s) difference of left forelimb minus right forelimb (n = 5 Thy1::ChR2 and 9 WT; n = 6 TSA-treated Thy1::ChR2 and 5 TSA-treated WT). (**C** and **D**) No alterations to paw pressure (C) or stride length (D) were observed in optogenetically-stimulated Thy1::ChR2 mice or their WT littermate controls. The same is true in animals treated with the histone deacetylase inhibitor trichostatin A (TSA) (C and D). Untreated: n = 5 Thy1::ChR2 mice and 9 WT mice. TSA-treated: n = 4 Thy1::ChR2 mice and 5 WT mice. n.s. indicates P value > 0.05. *P < 0.05. Error bars, SEM.